The Cosmic Microwave Background: Galactic Foregrounds and Faraday Rotation

Trey Connelly, Miguel Opena, Eric Frankel, Eric Ye, Luke Forsman, Adam Walker, Brian Zahn, and Paul McClernon

BASIS Scottsdale, Scottsdale, Arizona

Summary

This paper analyzes the cosmic microwave background (CMB) to determine the amount of influence each source of foreground contamination has on the microwave background measurements in relation to Faraday rotation. This study extends the analysis of Dineen and Coles, where the authors performed a novel analysis of the correlation between the Faraday rotation measure (RM), Wilkinson Microwave Anisotropy Probe (WMAP) sky maps, and CMB maps. Their technique has been replicated for numerous experiments analyzing the CMB. At the time, Dineen and Coles could only use a small Faraday RM dataset to test their hypothesis. With the advent of large, modern, and accurate Faraday rotation data, Dineen and Coles' hypothesis can be validated on a larger scale. We hypothesize that contaminated foreground maps will have more significant and complete cross-correlation with RM than determined by Dineen and Coles. Over 41,000 sources of new RM data were used, compared to the approximately 600 RM sources Dineen and Coles used, allowing for a more definite conclusion about the potential for contamination analysis in temperature maps. Ultimately, a strong correlation was found between the RM and unprocessed CMB maps, but not between RM and the foreground-removed CMB maps, demonstrating the value of cross-correlation between Faraday RM and CMB as a diagnostic for foreground contamination. These results support the conclusions drawn by Dineen and Coles.

Introduction

As the universe continues to expand, its mean energy content decreases as matter and radiation cools down (2). The mean kinetic energy of electrons also decreases until it can no longer overcome the electromagnetic attraction of protons; stable, neutral hydrogen atoms are then formed. This change of state initiated the age of recombination, believed to have taken place 370,000 years after the Big Bang (3). Since the age of recombination, the probability of interactions has been negligible, so protons move freely without ever colliding with each other. The consequence of this mechanism is that the universe is embedded uniformly in the cosmic microwave background (CMB), electromagnetic radiation that provides a picture of the universe's state nearly 13.7 billion years ago (4). The spectrum of the CMB is well-described by a blackbody function, which, by Planck's Law, relates the intensity of the CMB to the frequency of radiation emitted during recombination at 2.725 Kelvin, indicated in **Figure 1** (5).
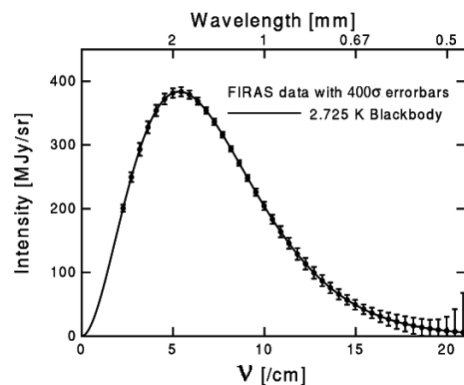

Figure 1: Measurement of the Cosmic Microwave Background from the COBE Satellite. Plotted with a blackbody function at 2.725 K, showing the intensity of the radiation produced as a function of frequency at a given temperature (3).

Anisotropies are observable irregularities in the temperature of the CMB, on the order of 10^{-5} Kelvin on both a global and a local scale throughout the universe (6). These small fluctuations are often difficult to measure due to the presence of foregrounds, localized sources of electromagnetic radiation which are much higher in intensity than the background and thus create significant interference (7). The three most significant foreground sources are synchrotron, free-free, and thermal dust emissions. Each foreground interferes with a particular range of electromagnetic frequencies; the highest-intensity ranges of each emission are 20-60 GHz, 50-60 GHz, and 100-200 GHz, respectively.

Synchrotron emission results from cosmic-ray

electrons accelerated in magnetic fields. For extreme relativistic electrons, the frequency spectrum is more complex and extends to many times the gyration frequency, or the frequency of the electron's revolution in a magnetic field. At low frequencies, synchrotron self-absorption is significant because for every emission process, there is a corresponding absorption process (8). Synchrotron emission also comes from radio spurs, the remnants of old supernovae explosions and the resulting shock fronts.

Free-free emission, also known as thermal Bremsstrahlung, arises from electron–ion scattering in interstellar plasma. The emission can be traced with hydrogen and α-particle line emission (9). Both types of emission come from singly-ionized hydrogen (HII) regions in the Galaxy (9). The intensity of free-free emission is given by an integration along the line of sight. Thermal free-free emission is intrinsically unpolarized because the scattering directions of electrons are isotropic and random (9). Some of the emitted radiation is self-scattered by electrons.

From 100 to 200 GHz, the foreground is dominated by thermal emission from interstellar dust grains, most of which are graphites, silicates, and polycyclic aromatic hydrocarbons (9). The temperature of the dust grain emission is determined by both interaction with interstellar radiation which excites the dust particles, producing heat, and the efficiency of radiation emission from the dust, which has a cooling effect (9).

While the Galactic plane, or the plane in which the majority of the Milky Way's mass lies, is largely the cause for foreground contamination, the interstellar medium has significant foreground contamination effects throughout the CMB. The interstellar medium consists of hot, low-density ionized gas, which fills 70-80% of Galactic volume. Interspersed within this gas are cold, neutral, dense clouds with high density of neutral hydrogen atoms (11). These dense neutral hydrogen regions often result in star formation, allowing for the possibility of changing into an ionized hydrogen zone (11). These clouds manifest in the CMB range of frequencies as a feature of the optical depth for the CMB radiation, creating negative spots around the clouds because high-energy electrons distort the CMB.

Faraday rotation is a magneto-optical phenomenon where an electromagnetic wave's plane of polarization is rotated while traveling through an external magnetic field. That rotation is linearly proportional to the component of the magnetic field in the direction of propagation (10). Because linear polarization can be decomposed into the superposition of two equal-amplitude circularly polarized components, this effect essentially rotates the orientation of a wave's linear polarization (10). Faraday rotation also manifests itself in the interstellar medium.

In this case, Faraday rotation is characterized by the difference in the refractive index experienced by the two circularly polarized propagation modes. Therefore, interstellar Faraday rotation (ß) is only dependent on the wavelength of light (λ). Faraday rotation is expressed as

$$\beta = RM\lambda^2$$

where RM denotes the rotation measure. This, in turn, is dependent on the axial component of the interstellar magnetic field and the number density of electrons along the propagation path,

$$RM = \frac{e^3}{8\pi^2\epsilon_0 m^2 c^3} \int_0^d n_e(s) B_|(s) ds$$

where e is the charge of an electron; ϵ_0 is the vacuum permittivity; m is the mass of an electron; c is the speed of light in a vacuum; $n_\epsilon(s)$ is the electron number density along path s; and $B_|(s)$ is the component of the interstellar magnetic field in the direction of propagation at each point s along the path. The integral is taken over the distance from the radiation source to the observer.

Faraday rotation measure (RM) is theoretically correlated to foreground contamination, and synchrotron and free-free foregrounds are correlated with the existence of a magnetic field as a result of cosmic ray acceleration and HII regions, respectively. Furthermore, magnetic fields are the source of Faraday rotation. To observe accurate measurements of the CMB, it is necessary to remove the contamination of Galactic noise caused by foregrounds, first by detecting when CMB measurements are contaminated. In 2003, Dineen and Coles demonstrated a method for analyzing the contamination of CMB maps using RM. With approximately 600 RM data points, they used novel methods of cross-correlation around neighborhoods of points in the CMB maps as a diagnostic for CMB contamination. They stated that a high cross-correlation of Faraday RM with CMB temperature differences could effectively indicate foreground contamination; however, they acknowledged that due to "the small size of our RM sample we used[,] these results are only suggestive" and that larger RM data sets would be needed for a more conclusive result (1).

In our analysis, we propose that the use of a newer, larger, and more accurate RM data set will lead to a more complete description of cross-correlation between foreground contamination and RM. We aim to analyze cross-correlation between RM and the three major foregrounds compared to cross-correlation between RM and the CMB maps. If our hypothesis is correct, it follows that the presence of foregrounds in CMB maps will be correlated with strong RM, allowing for more accurate assessment of the CMB. Our analysis makes use of CMB map data from the Wilkinson Microwave Anisotropy

Probe (WMAP) and Planck telescopes. Both surveys sought to map CMB anisotropies at the microwave and infrared scale, measuring the CMB as well as the various foregrounds. WMAP was operational from 2001 to 2010, and the Planck observatory was operational from 2009 to 2013.

Map	r_s	Correlation Probability	Map	r_s	Correlation Probability
Synchrotron			Synchrotron		
408 MHz (Unmasked)	0.366	1.00	408 MHz (Unmasked)	0.267	1.00
408 MHz (Masked)	0.257	1.00	408 MHz (COBE resolution)	0.277	1.00
K derived	0.324	1.00	408 MHz (Masked)	0.237	1.0o
Ka derived	0.324	1.00	K derived	0.289	1.00
Q derived	0.324	1.00	Ka derived	0.261	1.00
V derived	0.324	1.00	Q derived	0.196	1.00
W derived synchrotron map	0.324	1.00	V derived	0.168	1.00
Planck derived	0.369	1.00	W derived synchrotron map	0.094	0.99
Free-Free			Free-Free		
WMAP MEM (Unmasked)	0.390	1.00	Hα (Unmasked)	0.444	1.00
Planck derived	0.310	1.00	Hα (Masked)	0.496	1.00
			WMAP MEM (Unmasked)	0.427	1.00
Dust			Dust		
WMAP MEM (Unmasked)	0.295	1.00	FDS model (Unmasked)	0.405	1.00
Planck derived	0.446	1.00	FDS model (Masked)	0.429	1.00
			WMAP MEM (Unmasked)	0.247	1.00

Table 1: Significance of correlations of synchrotron, free-free, and dust foreground maps with Faraday rotation measures (left) versus the same from Dineen and Coles (1) (reproduced on right).

Results

The cross-correlation between the Opperman et al. Faraday rotation catalogs (12) and each sky map from the WMAP and Planck surveys was computed using the Spearman rank-order correlation coefficient, denoted r_s. The probability of a significant correlation was determined using Monte Carlo simulations, which attempt to remove any intrinsic correlation by shuffling the rotation measure values while keeping the source locations static. Dineen and Coles (1) used the same correlation algorithm, therefore our results are comparable. Using this method, the foreground maps have a correlation probability of 1.00 (**Table 1**, left). This indicates that there is a high likelihood of correlation between RM and the various foreground maps from synchrotron radiation, free-free radiation, and thermal dust emission.

For a CMB map, the resolution of the sample is expressed as N_{side}, which represents the number of partitions along a reference pixel to attain a specific resolution. For example, $N_{side} = 32$ denotes a need for 32 partitions along the side of a given reference pixel. This study's sample resolution is $N_{side} = 64$, versus foreground resolutions of 128, 256, and 512. The WMAP survey data was split into five bands of frequencies named K, Ka, Q, V, and W, corresponding to 22, 30, 40, 60, and 90 GHz, respectively. There is a likely correlation between the WMAP uncleaned sky maps and RM, as all five frequency bands have a correlation probability over 0.95. In contrast, the Internal Linear Combination (ILC) map, a combination of the five raw channels designed to minimize foregrounds, has an extremely low correlation probability (**Table 2**, left). The cross-correlation coefficients of the uncleaned maps are much higher and

Map	r_s	Correlation Probability	Map	r_s	Correlation Probability
			K	0.292	1.00
			Ka	0.189	1.00
K	0.349	1.00	Q	0.149	1.00
Ka	0.262	1.00	V	0.126	1.00
Q	0.213	1.00	W	0.063	0.95
V	0.151	1.00			
W	0.144	1.00	K (with mask)	0.296	1.00
K (with mask)	0.215	1.00	Ka (with mask)	0.099	0.97
Ka (with mask)	0.101	1.00	Q (with mask)	0.041	0.77
Q (with mask)	0.054	1.00	V (with mask)	0.049	0.81
V (with mask)	0.020	0.99	W (with mask)	0.043	0.78
W (with mask)	0.011	0.97			
			Internal linear combination map	0.021	0.71
Internal linear combination map	-0.0161	0.0002			
			TOH cleaned map	0.059	0.93
			TOH Wiener map	0.068	0.96

Table 2: Significance of correlations of maps resulting from the WMAP nine-year data with Faraday rotation measures (left) versus the WMAP one-year data from Dineen and Coles (1) (reproduced on right).

the cross-correlation coefficients of the cleaned map are much lower in this analysis than in Dineen and Coles' analysis of the WMAP data (**Table 2**, right), indicating that the more comprehensive RM data set is a better method of diagnosing foregrounds.

The results are similar for the Planck survey. The raw data maps of each frequency band are again significantly correlated with Faraday rotation measures (**Table 3**). When these maps are processed to form the various cleaned CMB maps (SMICA, Commander, NILC, and SEVEM), the resulting maps do not retain the correlation to Faraday rotation, falling short of a 0.95 correlation probability (**Table 4**). Thus, the processing of the CMB maps is effective in removing the Faraday rotation. The Planck consortium also produced confidence masks which remove regions of high contamination. When this mask is applied, the correlation values of the Planck maps decrease, again suggesting that the removal of foregrounds relates to the removal of correlation with RM. This mask is most effective in the NILC and SEVEM

Map	r_s	Correlation Probability
30 GHz	0.320	1.00
44 GHz	0.223	1.00
70 GHz	0.172	1.00
100 GHz	0.170	1.00
143 GHz	0.216	1.00
217 GHz	0.317	1.00
353 GHz	0.434	1.00
545 GHz	0.444	1.00
857 GHz	0.443	1.00

Table 3: Significance of correlations of maps from the Planck survey raw frequency channels with Faraday rotation measures.

Map	r_s	Correlation Probability
SMICA (Unmasked)	-0.001	0.08
SMICA (Masked)	-0.013	0.01
Commander (Unmasked)	-0.002	0.36
Commander (Masked)	-0.016	0.002
NILC (Unmasked)	0.002	0.66
NILC (Masked)	-0.009	0.05
SEVEM (Unmasked)	0.002	0.68
SEVEM (Masked)	-0.014	0.01

Table 4: Significance of correlations of maps from the Planck survey processed CMB maps with Faraday rotation measures.
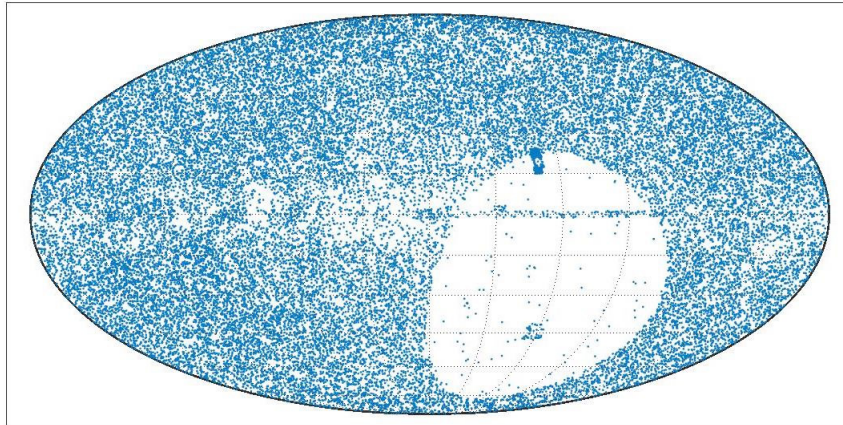
Figure 2: Sky Map. Of the sources of extragalactic Faraday rotation in Galactic coordinates. Each blue dot is a source.

maps, in which the correlation probability is decreased by more than 0.6.

Discussion

This paper sought to evaluate the 2004 Dineen and Coles study using new data gathered in the nine years after their publication. The central hypothesis to test was that a larger RM data set will lead to a more significant cross-correlation between foreground contamination and RM, allowing for the detection of such contamination. By cross-correlating RM data with the various sky maps, the likelihood for each map to have foreground contamination was determined. The pure foreground maps had a very high correlation value, empirically confirming the theoretical relationship between Faraday rotation and these foreground sources. The raw, uncleaned CMB maps in both WMAP and Planck had high correlation probabilities for all frequencies, while the processed, foreground-reduced maps from each survey had very low correlation probabilities. These results indicate a correlation between Faraday rotation and the presence of foreground radiation in a sky map.

As these results agree with the findings of Dineen and Coles (1), their method is thus shown to be valid for much more comprehensive RM data. The difference in correlation values between contaminated and clean data in our analysis is much greater than that in the original study. This seems to indicate that the RM test is not only valid for the larger RM data, but also more effective as a diagnostic. These results rely on RM data of about 41 thousand points across the CMB. Though a significant improvement from the Dineen and Coles study, this sample is still relatively small, as the foreground maps contained anywhere from 200 thousand to 3.1 million data points. Stronger results can be derived from future RM data with more points. Furthermore, having more data

points will also create a more accurate understanding of the RM phenomenon itself, indicating that future RM data can likely draw more detailed conclusions about the CMB.

Faraday rotation is not a phenomenon exclusive to foregrounds. Whereas this research examined Faraday rotation due to small-scale phenomena, research from other projects has been performed on primordial magnetic fields (PMFs), which persist throughout the galaxy. Unlike foregrounds caused by microscopic phenomena, these fields permeate the space around galaxies and galaxy clusters and affect the CMB in large-scale ways (3). Faraday rotation does occur as these fields interact with the CMB, indicating that future research could connect RM data to PMF data. As thermal dust is more strongly correlated with RM, thermal dust is potentially associated with a strong magnetic field. This trait of thermal dust is noted in Dineen and Coles (1), and the results corroborate the physical description of thermal dust as interacting strongly with PMFs (9). Such results indicate a crucial first step toward analyzing and understanding the CMB foregrounds, the complexities of which demand future research.

Methods

The Faraday rotation catalogs assembled by Oppermann *et al*. (12) were used to analyze correlation. This consists of 41,064 observationally estimated Faraday depths for extragalactic sources, including 124 sources from the catalog of Broten *et al*. (13) used by Dineen and Coles (1). The distribution of these sources covers nearly the entire Galactic sky (**Figure 2**). Note that the largest catalog, which contains the vast majority of data points, only examines the sky north of declination -40°; this causes the mostly empty area on the map.

The same measure of correlation used by Dineen and

Coles (2008), a Spearman rank-order correlation with significance determined by Monte Carlo simulations, was used for consistency between the two studies. The values of each rotation measure and temperature were replaced with their rank among all other rotation measures or temperatures in the sample, from 1 to the total number of sources (41,064). Tied values are assigned the average rank of the values. Note that only the intensities of temperature measurements and rotation measures are compared; the signs of the rotation measures are ignored. The Spearman rank-order correlation coefficient, r_s, is given by

$$r_s = \frac{\sum_i (x_i - \bar{x})(y_i - \bar{y})}{\sqrt{\sum_i (x_i - \bar{x})^2}\sqrt{\sum_i (y_i - \bar{y})^2}}$$

where x_i is the rank of the temperature T_i among all N temperature values and y_i is the rank of the temperature R_i among all rotation measures.

This coefficient is a measure of a monotonic relationship between temperature and RM. A value of 1 represents a perfectly monotonically increasing relationship (*i.e.* as temperature increases, RM strictly increases), whereas a value of -1 represents a perfectly monotonically decreasing relationship (*i.e.* as temperature increases, RM strictly decreases).

Monte Carlo simulations were used to determine the significance of the correlation coefficients. Ten thousand Monte Carlo simulations were performed, where the rotation measures were unlinked from temperature values by randomly shuffling the rotation measures among the sources while preserving the source locations. The significance of the correlation coefficients is thus the fraction of the simulated correlation values that are less than the real value.

Dineen and Coles (1) analyze eight synchrotron foreground maps in order to verify a correlation between synchrotron emission and rotation measures, the Haslam *et al*. (14) 408 MHz survey and five maps produced from the first-year WMAP data. The synchrotron maps analyzed in this paper are the 408 MHz data, the five updated synchrotron maps produced by the WMAP team (15) using the nine-year WMAP data and the same maximum entropy method (MEM) as the first-year maps, and a map produced by the Planck Collaboration using an astrophysical component separation analysis that combines Planck observations, the Haslam *et al*. survey, and the nine-year WMAP data (16). The Haslam *et al*. map and all WMAP-derived maps are found in the NASA archive (18), and all Planck maps can be retrieved from the ESA Planck Legacy Archive (19). All maps are produced in HEALPix format, the WMAP foregrounds at resolution parameter N_{side}=128, the 408 MHz map at N_{side}=512, and the Planck foregrounds at N_{side}=256.

In revisiting the relationship between free-free radiation and RM, three maps were used: the nine-year version of the WMAP map once more; a free-free map at the K-band frequency produced using the MEM approach; and the free-free map produced by the Planck team using the same component separation analysis. For dust, two additional maps were used: one produced from the nine-year WMAP team using MEM at the W-band frequency, and the other by the Planck team using component separation analysis. The synchrotron, free-free, and dust foreground maps were analyzed (**Table 1**, left) and generally displayed increased cross-correlation compared to the analysis from Dineen and Coles (**Table 1**, right).

The WMAP instrument collected intensity data from ten 4-channel radiometer assemblies measuring over five frequency bands. The K, Ka, Q, V, and W bands roughly correspond to 22, 30, 40, 60, and 90 GHz, respectively. The WMAP team also created an Internal Linear Combination (ILC) map formed from a weighted linear combination of the five smoothed intensity maps in which the weights are chosen to maintain the CMB anisotropy signal while minimizing the Galactic foreground contribution.

CMB analysis also involves masks which remove regions of high foreground contamination in order to better isolate the microwave background. The kq85 mask for WMAP data, removing 25.2% of the measurements, was used for its standing as convention and its rough equivalence to the "Kp2" cut in the 1-year and 3-year releases. When this mask is applied, 32881 of the 41064 RM sources remain available for analysis. The five WMAP frequency channel maps, masked and unmasked, and the ILC map were correlated with RM, showing high correlation probabilities for all maps except the ILC map (**Table 2**, left).

The Planck satellite contains two main instruments for measuring intensity over nine frequency channels, the Low Frequency Instrument (LFI) and the High Frequency Instrument (HFI). The LFI consists of 11 radiometers in the Ka, Q, and V bands, with center frequencies close to 30, 44, and 70 GHz, and is available at N_{side}=256. The HFI is designed around 52 bolometers covering six bands centred at 100, 143, 217, 353, 545, and 857 GHz, available at N_{side}=2048 (**Table 3**).

The Planck Collaboration provides four different methods for separating CMB from foreground components using the nine channels of Planck data, as detailed in (17). Note that the COMMANDER method also incorporates data from WMAP and the Haslam *et al*. (14) 408 MHz survey. A common mask is also provided, consisting of the union of confidence masks of the Commander, SEVEM, and SMICA separation methods, removing 22.4% of the measurements. These four methods were analyzed, using both masked and

unmasked sets of data (**Table 4**). When using this mask, 31,756 Faraday rotation sources remain available for analysis.

References

1. Dineen P and Coles P. "Faraday Rotation as a Diagnostic of Galactic Foreground Contamination of Cosmic Microwave Background Maps." *Monthly Notices of the Royal Astronomical Society* 347.1 (2004): 52-58.
2. Cabella P and Marinucci P. "Statistical Challenges in the Analysis of Cosmic Microwave Background Radiation." *Annals of Applied Statistics* 3.1 (2009): 61-95.
3. CMB Collaboration. "CMB-S4 Science Book, First Edition." *ArXiv Preprint*, 2016. Web.
4. White M, Krauss LM, Silk J. "Cosmic Variance in CMB Anisotropies: From 1° to COBE." *Astrophysics Journal* 1.1 (1993): 418-535.
5. Scott D and Smoot GF. "Cosmic Microwave Background." *ArXiv Preprint*, 2010. Web.
6. Elsner F and Wandelt BD. "Likelihood, Fisher Information, and Systematics of Cosmic Microwave Background Experiments." *Astronomical Astrophysics* 542 (2012): A60.
7. Sehgal N, Madhavacheril MS, Sherwin B, van Engelen A. "Internal Delensing of Cosmic Microwave Background Acoustic Peaks." *ArXiv Preprint*, 2016. Web.
8. Smoot GF. Synchrotron Radiation as CMB Foreground. *ArXiv Preprint*, 1999. Web.
9. Ichiki K. "CMB Foreground: A Concise Review." *Progress of Theoretical and Experimental Physics* 6.1 (2014).
10. De S, Pogosian L, Vachaspati T. "CMB Faraday Rotation as Seen through the Milky Way." *ArXiv Preprint*, 2013. Web.
11. Hansen M, Zhao W, Frejsel AM, Naselsky PD, Kim J, Verkhodanov OV. "Faraday Rotation as a Diagnostic of Galactic Foreground Contamination of CMB Maps." *MNRAS* 426.1 (2012): 57-69.
12. Oppermann N, *et al*. "Estimating Extragalactic Faraday Rotation." *A&A* 575 (2015): A118.
13. Broten NW, MacLeod JM, Vallée JP. "Catalogue of Unambiguous (Faraday-thin, One-component, Spectrum-selected) Rotation Measures for Galaxies and Quasars." *Astrophysics and Space Science* 141.2 (1988): 303-331.
14. Haslam CGT, Salter CJ, Stoffel H, Wilson WE. "A 408 MHz All-Sky Continuum Survey. II-The Atlas of Contour Maps." *Astronomy and Astrophysics Supplement Series* 47 (1982): 1.
15. Bennett CL, *et al*. "Nine-year Wilkinson Microwave Anisotropy Probe (WMAP) Observations: Final Maps and Results." *The Astrophysical Journal Supplement Series* 208.2 (2013): 20.
16. Planck Collaboration. "Planck 2015 Results. X. Diffuse Component Separation: Foreground Maps." *A&A* 594 (2016): A10.
17. Planck Collaboration. "Planck 2015 Results. IX. Diffuse Component Separation: CMB Maps." *A&A* 594 (2016): A9.
18. Legacy Archive for Microwave Background Data Analysis. NASA Goddard Space Flight Center. Web. URL: https://lambda.gsfc.nasa.gov.
19. Planck Legacy Archive. ESA European Space Astronomy Centre. Web. URL: http://pla.esac.esa.int.